Intra-operative Update of Neuro-images: Comparison of Performance of Image Warping Using Patient-Specific Biomechanical Model and BSpline Image Registration

Ahmed Mostayed, Revanth Reddy Garlapati, Grand Roman Joldes, Adam Wittek, Ron Kikinis, Simon K. Warfield, and Karol Miller

Abstract This paper compares the warping of neuro-images using brain deformation predicted by means of patient-specific biomechanical model with the neuro-image registration using BSpline-based free form deformation algorithm. Deformation fields obtained from both algorithms are qualitatively compared and overlaps of edges extracted from the images are examined. Finally, an edge-based Hausdorff distance metric is defined to quantitatively evaluate the accuracy of registration for these two algorithms. From the results it is concluded that the patient-specific biomechanical model ensures higher registration accuracy than the BSpline registration algorithm.

A. Mostayed (✉) • R.R. Garlapati • G.R. Joldes • A. Wittek
Intelligent Systems for Medicine Laboratory, The University of Western Australia, Perth, Australia
e-mail: mostayed@mech.uwa.edu.au; revanth@mech.uwa.edu.au; grandj@mech.uwa.edu.au; adwit@mech.uwa.edu.au

R. Kikinis
Surgical Planning Laboratory, Brigham & Women's Hospital, Harvard Medical School, Boston, MA, USA
e-mail: kikinis@bwh.harvard.edu

S.K. Warfield
Computational Radiology Laboratory, Children's Hospital, Harvard Medical School, Boston, MA, USA
e-mail: Simon.Warfield@childrens.harvard.edu

K. Miller
Intelligent Systems for Medicine Laboratory, The University of Western Australia, Perth, Australia

Institute of Mechanics and Advanced Materials, Cardiff School of Engineering, Cardiff University, Wales, UK
e-mail: kmiller@mech.uwa.edu.au

A. Wittek et al. (eds.), *Computational Biomechanics for Medicine: Models, Algorithms and Implementation*, DOI 10.1007/978-1-4614-6351-1_12,

1 Introduction

In a neurosurgical procedure the aim of a surgeon is to resect as much diseased tissues as possible while preserving healthy tissues. Sophisticated pre-operative imaging techniques have been developed over the past decade to aid neurosurgeons with improved visualization [1]. However, surgical interventions (craniotomy, for example) tend to distort the pre-operative anatomy and often lead to misalignment between the actual position of pathology and its position determined from pre-operative images [2]. In addition, constraints of the operating room restrict the contrast and resolution of intra-operative images. These barriers, in principle, can be overcome by aligning high quality pre-operative scans to intra-operative ones. Accurate alignment demands that the pre-operative image is non-rigidly registered with the intra-operative image.

The field of non-rigid registration of medical images has evolved in two separate streams. One way to register the pre-operative image with the intra-operative image is to use some intensity-based similarity criterion and derive a non-linear warp function, which then can be used for warping the pre-operative image. In this approach images are often treated as fluids or elastic bodies subjected to elastic deformation [3]. The similarity criterion acts as the driving force of the deformation. The BSpline-based free form deformation (FFD) algorithm [4] is considered as a state-of-the-art non-rigid registration algorithm belonging to this category. However, BSpline registration algorithm may often produce physically implausible deformation field [5].

On the other hand it is shown in [2, 6–10] that the craniotomy-induced brain shift can be predicted by non-linear biomechanical models. These models take into account the mechanical behaviour of different classes of brain tissue (ventricle, parenchyma, and tumour) and do not need a similarity criterion to drive the numerical computation. In fact, the need for a target image (intra-operative image in this case) can be eliminated and numerical computation can be carried out with only the knowledge of the displacement of few points on the brain surface near craniotomy.

In this work, the non-rigidly registered pre-operative images obtained using deformations within the brain predicted by means of both a biomechanical model [2, 6] and a BSpline algorithm implemented in 3D Slicer (www.slicer.org) are analyzed and compared. For five different patients undergoing surgery, the accuracy of registration is compared both qualitatively and quantitatively. The deformation fields obtained from each registration algorithm are qualitatively compared. Also the amount of overlap between edge contours obtained from the registered pre-operative image and the edge contours of the intra-operative image is compared for both registration algorithms. Finally, a novel edge-based Hausdorff distance (HD) measure is used to compare the results quantitatively.

2 Registration Methods

2.1 Image Data

Five surgery cases involving tumour resection were analysed in this work. They were used for biomechanical model-based warping in previous studies carried out in [2] and [6]. For each case a high resolution, high quality pre-operative image and a low resolution intra-operative image were available. For the purpose of this paper the preoperative image for each case is registered with its corresponding intra-operative image using both the biomechanical model and the BSpline registration algorithm. The pre-operative images have a resolution of $256 \times 256 \times 124$ voxels and the intra-operative images have a resolution of $256 \times 256 \times 60$ voxels. Voxel size for the pre-operative image is $0.9375 \times 0.9375 \times 1.3\,\text{mm}^3$ and for the intra-operative image $0.8594 \times 0.8594 \times 2.5\,\text{mm}^3$.

2.2 Image Warping Using Intra-operative Brain Deformations Predicted from Patient-Specific BiomechanicalModel

Construction of patient-specific finite element mesh. A three-dimensional (3D) surface model of each patient's brain was created from segmented pre-operative magnetic resonance image (MRI). A brain mesh was constructed from the surface model with 8-noded hexahedral and 4-noded tetrahedral elements. The meshes were generated using IA-FEMesh (University of Iowa [11]) and HyperMesh (commercial FE mesh generator by Altair of Troy, MI, USA).

Loading and boundary conditions. The displacements were applied on the exposed part (due to craniotomy) of the brain surface. In [12] it is suggested that for this type of loading the unknown deformation field within the brain very weakly depends on the constitutive model. The displacements for loading the models were determined from the segmented pre-operative and intra-operative cortical surfaces. The correspondence between pre-operative and intra-operative cortical surface was determined by applying the Vector-Spline regularization algorithm [13] to the surface curvature maps. In order to define the boundary condition for the unexposed nodes on the brain surface, a contact interface was defined between the rigid skull model and that part of the brain. The frictionless sliding contact proposed in [14] is used which prevents the brain from penetrating the skull.

Mechanical properties. According to [12] if geometric nonlinearity is considered, the results of prediction of deformation field within the brain shift are only weakly affected by the constitutive model of the brain tissue. Therefore, a simple Neo-Hookean model was used [15]. The Young's modulus of 3,000 Pa was selected for parenchyma [16]. The Young's modulus for tumour was assigned two times larger than for parenchyma. Poisson's ratio 0.49 was chosen for the parenchyma and tumour following [2].

Algorithm. An efficient algorithm for integrating the equations of solid mechanics has been developed by Joldes et al. [17–19]. The computational efficiency of this algorithm is achieved by using—(1) Total Lagrangian (TL) formulation [17] for updating the calculated variables; and (2) Explicit Integration in the time domain combined with mass proportional damping. In the TL formulation, all the calculated variables (such as displacements and strains) are referred to the original configuration of the analysed continuum [18]. The decisive advantage of this formulation is that all derivatives with respect to spatial coordinates can be pre-computed [17]. In explicit time integration, the displacement at time $t + \Delta t$(where Δt is the time step) is solely based on the equilibrium at time t. Therefore, no matrix inversion and iterations are required when solving nonlinear problems. Application of explicit time integration scheme reduces the time required to compute the brain deformations by an order of magnitude in comparison with implicit integration typically used in commercial finite element codes [2].

Image warping. At first the pre-operative image is aligned with the intra-operative image using rigid registration. In order to obtain the warped pre-operative image, the coordinate of each voxel of the discrete image grid has to be mapped onto the original (un-deformed) pre-operative image grid. To perform such mapping, the deformed (when predicting the deformation within the brain) and un-deformed (corresponding to the pre-operative brain geometry) brain meshes are first re-meshed by Delaunay tessellation. Then the enclosing tetrahedral element for each voxel is found using the Quick–Hull algorithm [20]. The coordinate of a particular voxel in the original pre-operative image grid is determined by using the shape functions of its enclosing tetrahedron. The intensity value of the voxel is interpolated from the intensity value of its neighbours by using tri-cubic interpolation [21]. All these tasks are performed using an in-house code programmed in MATLAB^{TM}.

2.3 BSpline Registration

BSplines are bell-shaped functions that were introduced by Schoenberg [22] for interpolation. Due to their minimal local support they have become a strong tool for modelling 3D deformable shapes. BSplines are useful for both interpolation and approximation of scattered data. Free-form-deformation (FFD) based on BSpline algorithm is widely used for non-rigid image registration [3]. The initial algorithm proposed by Rueckert et al. [4] was based on the multi-level BSpline approximation algorithm (MBA) developed by Lee et al. [23] for scattered data interpolation. The basic idea of FFD is to deform an object by manipulating an underlying mesh of control points. The resulting deformation controls the shape of the 3D object and produces a smooth transformation. The FFD algorithm maximizes the mutual information [24] between the pre-operative and intra-operative image to obtain the warping transform. A regular grid of control points with equal spacing is required.

For highly localized non-rigid deformations, which can be expected in neurosurgery, a high resolution control grid needs to be used. The resolution also defines the number of degrees of freedom (DoF) of the transformation, for example a $10 \times 10 \times 10$ grid of control points yields a transformation with $3 \times 10 \times 10 \times 10$ DoFs in 3D.

The BSpline transform for the analysed neurosurgery cases were obtained by the BSpline registration module of 3D Slicer v3.6. The initial size of the BSpline grid was $10 \times 10 \times 10$. Fifty histogram bins and 10,000 spatial samples were used to calculate the marginal and joint entropies [25]. Total number of iterations was selected as 20. The similarity criterion of this Slicer module is based on Mattes mutual information [25].

3 Qualitative Comparison

3.1 Deformation Field

The deformation fields predicted by the biomechanical model and the deformation field obtained from the BSpline transform are compared in Fig. 1. These deformation fields are three dimensional. However, for clarity, only arrows representing 2D vectors (x and y component of displacement) are shown overlaid on the un-deformed pre-operative slices. Each of these arrows represents the displacement of a voxel of the pre-operative image domain.

The deformation fields predicted by the biomechanical model is very similar to the one calculated from the BSpline registration for case 1. For this case the maximum deformation of the surface of the brain was approximately 4 mm. However, for case 2 deformation predicted by the biomechanical model significantly differs from that obtained using BSpline registration. For this case the maximum deformation of the brain surface was around 8 mm. For cases 3 and 5, the maximum deformation of the brain surface was between 4 and 5 mm. For these two cases, the deformation fields from the biomechanical model and BSpline registration are similar in the craniotomy and tumour areas, but look significantly different in other parts of the brain. For case 4, the deformation fields predicted using the two methods differ significantly near the craniotomy.

3.2 Canny Edges

Plot of deformation vectors provides useful estimate of the nature of non-rigid transform between two images. However, to obtain a qualitative assessment of the degree of alignment after registration, one must examine the overlap of corresponding anatomical features of the intra-operative and registered pre-operative

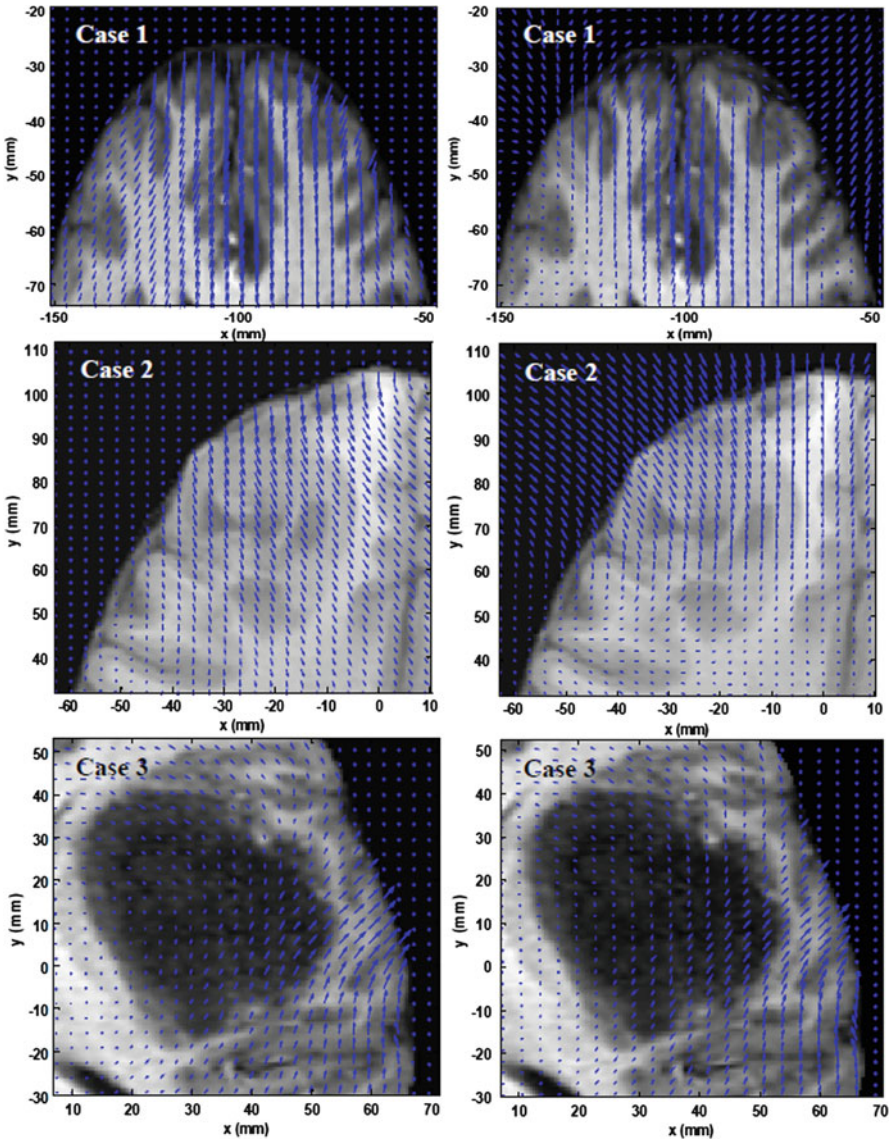

Fig. 1 The predicted deformation fields overlaid on an axial slice of pre-operative image. An arrow represents a 2D vector consisting of the x (R–L) and y (A–P) components of displacement at a voxel centre. Left column: deformation field predicted by biomechanical warping. Right column: deformation field derived from BSpline registration transform. The predicted deformation fields overlaid on an axial slice of pre-operative image. Left column: deformation field predicted by biomechanical warping. Right column: deformation field derived from BSpline registration transform

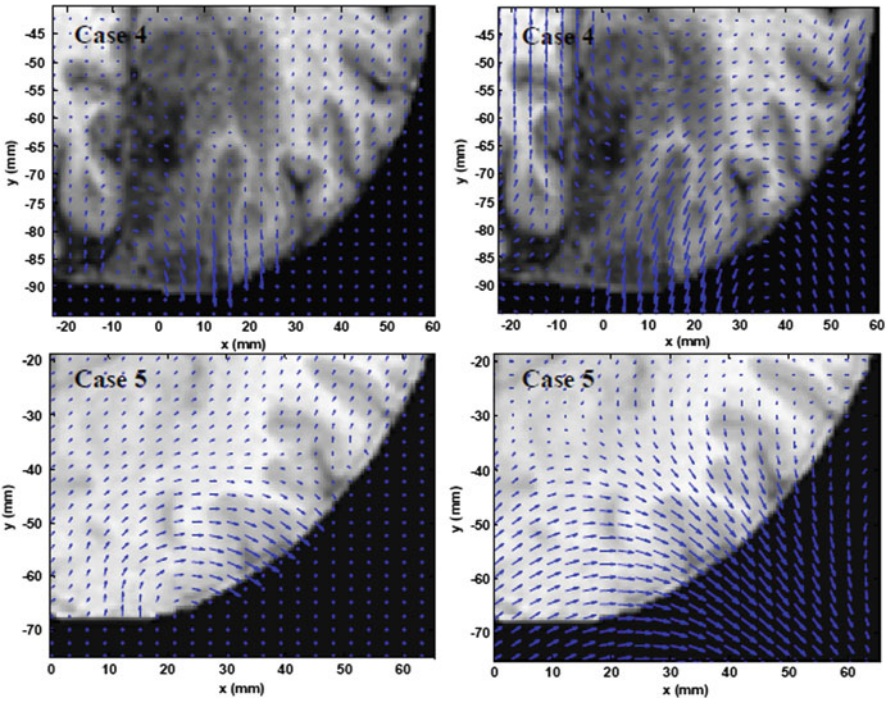

Fig. 1 (continued)

image. For this purpose tumours and ventricles in both registered pre-operative and intra-operative images can be segmented and their surfaces can be compared [6]. Image segmentation is time consuming, not fully automated and not suitable for comparing a large number of image pairs [26]. Therefore in this study, we use edges detected from an image. Such edges are regarded as useful and easily recognizable features, and they can be detected using techniques that are totally automated and fast. Hence, Canny edges [27] obtained from the intra-operative and registered pre-operative image slices are labelled in different colours and overlaid (Fig. 2). In Fig. 2 intra-operative edges are labelled with blue and pre-operative edges are represented with red and their overlap pixels are labelled in green.

From Fig. 2 we can see that misalignments between the edges detected from the intra-operative images and the edges from the pre-operative images updated to the intra-operative brain geometry are much lower for the biomechanics-based warping than for BSpline registration. The edges obtained from the images warped with both registration algorithms are similar for cases 1, 4, and 5. It is related to the fact that the deformation fields predicted using our biomechanical model and BSpline registration are very similar for these three cases. However, as indicated by visual inspections, for case 2, misalignment between the edges obtained from the intra-operative image and edges from the pre-operative image registered using

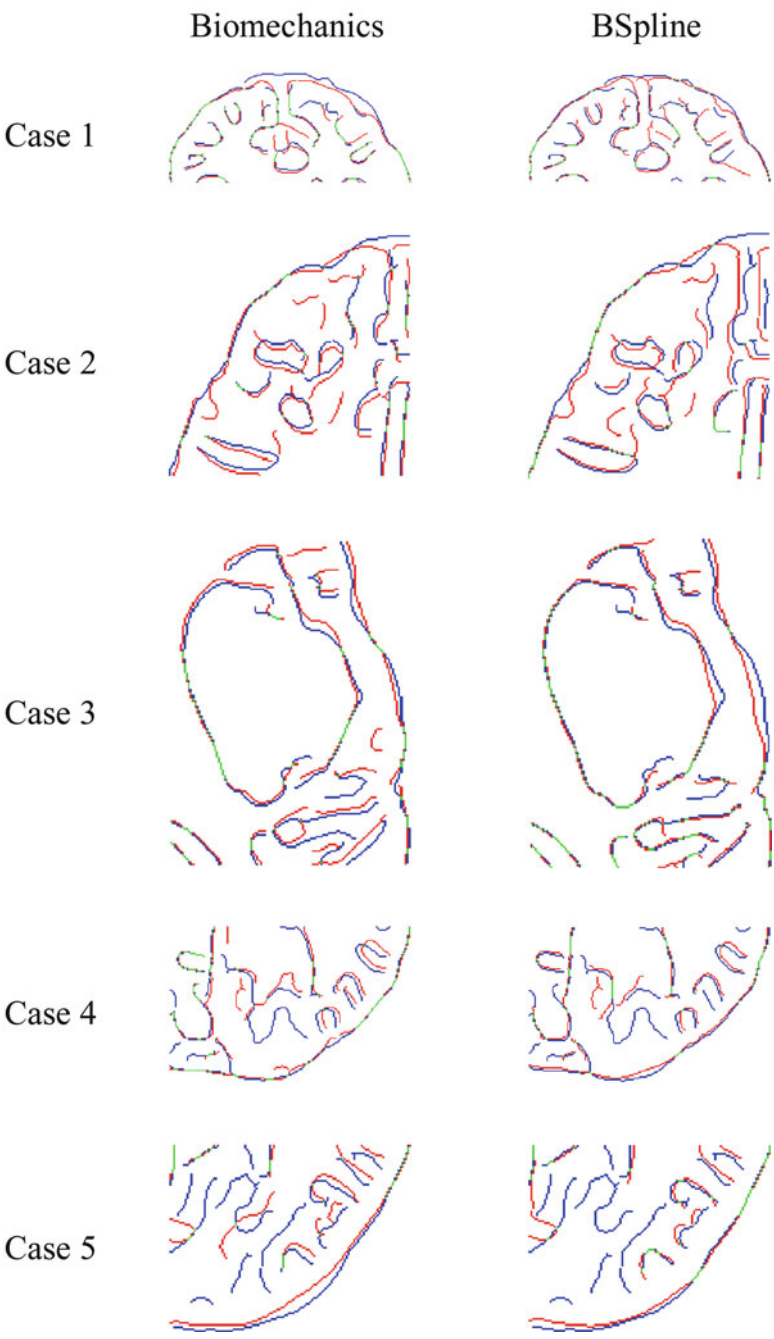

Fig. 2 Canny edges extracted from intra-operative and the registered pre-operative image slices overlaid on each other. Blue colour represents the non-overlapping pixels of the intra-operative slice and red colour represents the non-overlapping pixels of the pre-operative slice. Green colour represents the overlapping pixels. Left column: edges of the deformed pre-operative image obtained by applying biomechanical warping. Right column: edges of the deformed pre-operative image obtained by applying BSpline registration algorithm

BSpline algorithm can be observed. For this case there was a large intra-operative brain shift and the deformation field obtained using BSpline algorithm significantly differ from deformation predicted using biomechanical model. It is an indication that the BSpline registration algorithm cannot perform as well as the biomechanics warping if large deformation is involved. In Sect. 4 the misalignment between edges is quantified using a novel edge-based Hausdorff distance measure [28].

4 Quantitative Comparison

4.1 Edge-based Hausdorff Distance

We begin the section with a definition of the traditional point-based Hausdorff distance (HD) between two intensity images $\mathbf{I}$ and $\mathbf{J}$. Let I and be J the binary edge images derived from $\mathbf{I}$ and $\mathbf{J}$, respectively, and $\mathbf{A} = \{a_1, \cdots, a_n\}$ and $\mathbf{B} = \{b_1, \cdots, b_n\}$ are the set of non-zero points corresponding the non-zero pixels on the edge images, then the directed distance between them $h(\mathbf{A}, \mathbf{B})$ is defined as the maximum distance from any of the points in the first set to the second one:

$$h(\mathbf{A}, \mathbf{B}) = \underset{a \in \mathbf{A}}{\operatorname{argmax}} \left[\underset{b \in \mathbf{B}}{\operatorname{argmin}} \|a - b\|_2 \right] \tag{1}$$

$$h(\mathbf{B}, \mathbf{A}) = \underset{b \in \mathbf{B}}{\operatorname{argmax}} \left[\underset{a \in \mathbf{A}}{\operatorname{argmin}} \|b - a\|_2 \right] \tag{2}$$

The HD between the two sets $H(\mathbf{A}, \mathbf{B})$ is defined as the maximum of these two directed distances:

$$H(\mathbf{A}, \mathbf{B}) = \max\left(h(\mathbf{A}, \mathbf{B}), h(\mathbf{B}, \mathbf{A})\right) \tag{3}$$

The proposed directed distance between two sets of edges is defined as

$$h_e(\mathbf{A}^e, \mathbf{B}^e) = \underset{a_i^e \in \mathbf{A}^e}{\operatorname{argmax}} \left[\underset{b_j^e \in \mathbf{B}^e}{\operatorname{argmin}} \left\| a_i^e - b_j^e \right\| \right] \tag{4}$$

where $\mathbf{A}^e = \{a_1^e, \cdots, a_m^e\}$ and $\mathbf{B}^e = \{b_1^e, \cdots, b_n^e\}$ are two sets of edges.

The quantity $\|a_i^e - b_j^e\|$ in Eq. (4) is nothing but the point-based Hausdorff distance between two point sets $\mathbf{M} = \{m_1 \cdots, m_p\}$ and $\mathbf{T} = \{t_1 \cdots, t_q\}$ representing edges a_i^e and b_i^e, respectively,

$$\left\| a_i^e - b_j^e \right\| := d(a_i^e - b_j^e) = \max\left(h(\mathbf{T}, \mathbf{M}), h(\mathbf{M}, \mathbf{T})\right) \tag{5}$$

Now the edge-based Hausdorff distance is defined as

$$H_e(\mathbf{A}^e, \mathbf{B}^e) = \max\left(h_e(\mathbf{A}^e, \mathbf{B}^e), h_e(\mathbf{B}^e, \mathbf{A}^e)\right) \tag{6}$$

Fig. 3 Overlaid edges before (left) and after (right) round-trip consistency. Blue colour represents the non-overlapping pixels of the intra-operative slice and red colour represents the non-overlapping pixels of the pre-operative slice. Green colour represents the overlapping pixels

Pre-processing. Some pre-processing of the extracted edges was required before the edge-based Hausdorff distance could be calculated. Some small misalignments between the edges detected from two images are inevitable even after the registration. The pre-processing step finds the pixels of one image that are most likely to have correspondence with the other image. For each non-zero pixel involved in the binary edge image, A, the closest non-zero pixel in the other image, B, is found. The same procedure is repeated from this pixel in image B to find the closet non-zero pixel in image A. One would reach the starting point, if the images were perfectly aligned. However, in reality, the images are not perfectly aligned. Hence, we often end up at a point that is different from the starting point in image A. The distance between the starting point and end point in image A is termed the "round-trip distance". The pixels that have a round trip distance greater than a prescribed threshold (referred to as "round-trip threshold") are excluded (see Fig. 3), as they are less likely to have correspondence with any pixel in the other image. The higher the threshold; the lower the consistency between the pixels. However, excessively low value of this threshold can cause removal of important feature points. Hence, it is crucial to select an optimal threshold that maximizes the consistency and minimizes the number of features removed. Throughout this paper a threshold of 1.5 mm is used. The round-trip consistency procedure tends to generate artefacts by eliminating points in the interior of an edge which results in several broken edges. Such edge pixels are recovered by applying morphological filters [21]. Any edge shorter than 5 mm was removed from the images before maximizing the consistency using round-trip consistency criterion as their dimension is insignificant compared to the relevant brain dimension.

Methodology. For the quantitative evaluation of registration accuracy, each image volume was cropped into a region-of-interest (ROI) which encloses the tumour. These ROI sub-volumes were re-sliced (in the axial plane) with a slice thickness of 1.45 mm and the in-plane resolution was increased to $0.5 \times 0.5\,\text{mm}^2$. This was done to improve the precision of Canny edge detection [27] used in a slice-by-slice registration accuracy evaluation process. The proposed edge-based Hausdorff distance (HD) was used to calculate the misalignment between slice pairs. The directed distances for all edge pairs [see Eq. (4)] are recorded and the edge-based

Hausdorff distance values at different percentile of directed distances are plotted (see Fig. 4). The *P*th percentile HD, "D", between two images means that "*P*" percent of edge pairs have a Hausdorff distance below D.

4.2 Results

The percentile vs. Hausdorff distance (HD) curve provides an estimation of the percentage of edges that were successfully registered in the registration process (Fig. 4). As accuracy of the edge detection is limited within the image resolution, an alignment error twice the in-plane resolution of the intra-operative image (which is 0.8594 mm for the five cases considered) cannot be avoided. Hence, for five cases analysed here, any edge pair having HD value less than 1.7 mm can be considered successfully registered. It is obvious from Fig. 4 that biomechanical warping was able to successfully register more edges than the BSpline registration for all five cases.

Percentile of edges successfully registered by two registration algorithms (i.e. warping using biomechanical model and BSpline registration) for each analysed case is listed in Table 1. It can be clearly seen from this table that the percentile of successfully registered edge is higher for image warping using biomechanical model than for BSpline registration.

For all five cases, the percentiles vs. HD curves tend to rise steeply around 90 percentile. Hence, it can be safely assumed that edge pairs that do not have any correspondence (outliers) are between 91 and 100 percentile. The 90-percentile HD values for five cases are listed in Table 2.

5 Discussions

From the results presented in Sects. 3 and 4 it is evident that application of the intra-operative deformation predicted using patient-specific biomechanical model [2, 6] to warp pre-operative images ensures higher registration accuracy than BSpline-based image registration [4]. Biomechanical models are especially effective in neurosurgery cases where intra-operative brain shift is large. Another distinctive advantage of the biomechanical algorithm is that it does not need the intra-operative image at all to compute deformation. Only the displacement of a limited number of points on the exposed (during craniotomy) intra-operative brain surface is required. Such displacement can be determined from 3D ultrasound or 3D laser range imaging [29].

For image warping using the intra-operative brain deformation predicted from patient-specific biomechanical model, the required amount of intra-operative data points is reduced to a few hundred compared to few millions for BSpline registration (Table 3).

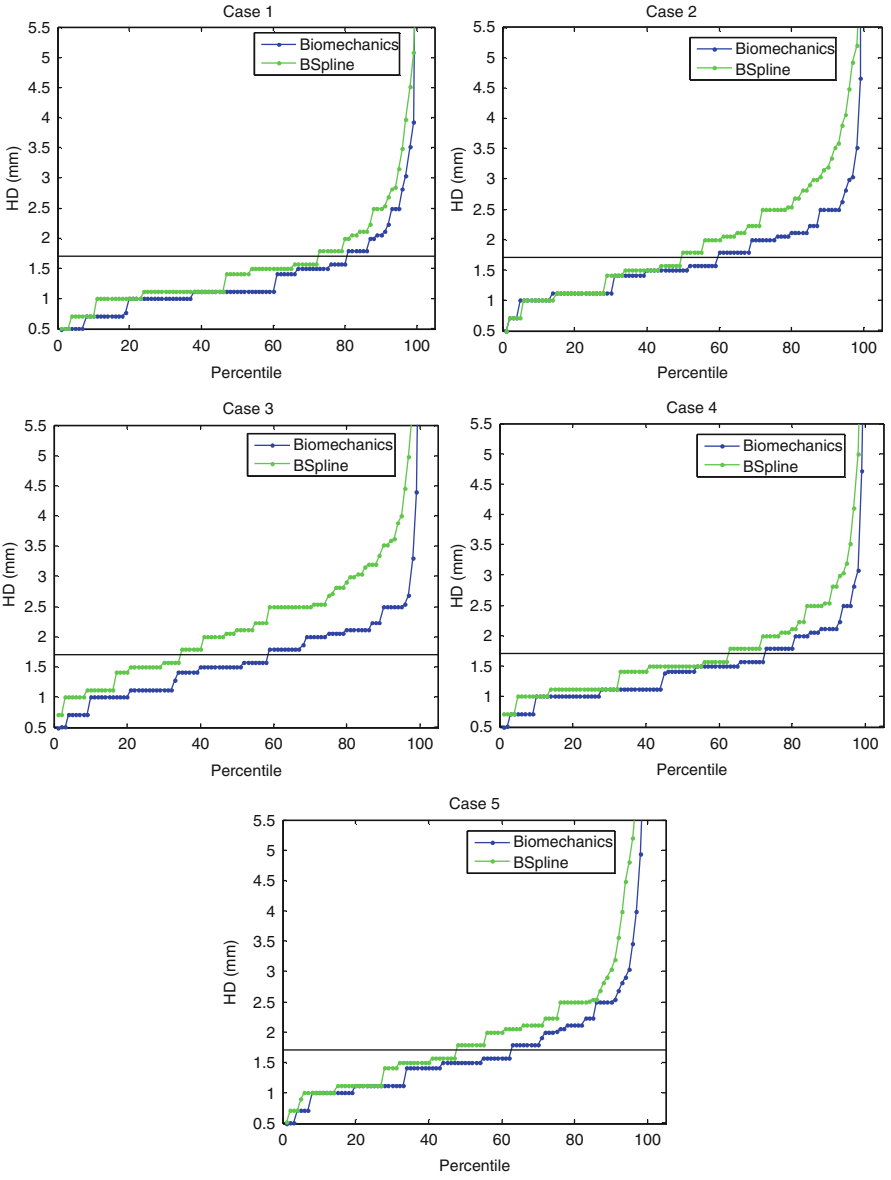

Fig. 4 The plot of Hausdorff distance between intra-operative and registered pre-operative images against the percentile of edges. The horizontal line is the 1.7 mm mark

Table 1 Percentile of edges successfully registered for five patient specific cases

	Percentile of edges successfully registered	
Case	Biomechanics	BSpline
'1'	80	72
'2'	59	49
'3'	58	34
'4'	72	62
'5'	62	47

Table 2 90 percentile Hausdorff distance values for five patient specific cases

	Non-rigid registration algorithm	
Case	Biomechanics	BSpline
'1'	2.06 mm	2.49 mm
'2'	2.49 mm	3.19 mm
'3'	2.49 mm	3.52 mm
'4'	2.11 mm	2.54 mm
'5'	2.49 mm	3.03 mm

Table 3 Number of points of intra-operative geometry required for numerical computation

	Data requirement (No. of points)	
Case	Biomechanics	BSpline
'1'	322	3.932×10^6
'2'	328	3.932×10^6
'3'	171	3.932×10^6
'4'	134	3.932×10^6
'5'	63	3.932×10^6

The presented results of comparison of warping of neuro-images using brain deformation predicted by means of patient-specific biomechanical model with the BSpline-based neuro-image registration were obtained using the BSpline algorithm implemented in 3D Slicer. An alternative implementation and alternative algorithms for image-based alignment should be evaluated in future work.

Acknowledgements The first author is a recipient of the SIRF scholarship and acknowledges the financial support of the University of Western Australia. The financial support of National Health and Medical Research Council (Grant No. APP1006031) is gratefully acknowledged. This investigation was also supported in part by NIH grants R01 EB008015 and R01 LM010033 and by a research grant from the Children's Hospital Boston Translational Research Program. In addition, the authors also gratefully acknowledge the financial support of Neuroimage Analysis Center (NIH P41 EB015902), National Center for Image Guided Therapy (NIH U41RR019703) and the National Alliance for Medical Image Computing (NAMIC), funded by the National Institutes of Health through the NIH Roadmap for Medical Research, Grant U54 EB005149. Information on the National Centers for Biomedical Computing can be obtained from http://nihroadmap.nih.gov/bioinformatics.

References

1. Warfield, S.K., Haker, S.J., Talos, I.F. et al.: Capturing intraoperative deformations: research experience at Brigham and Women's hospital. Med. Image Anal. **9**, 145–162 (2005)
2. Wittek, A., Miller, K., Kikinis, R. et al.: Patient specific model of brain deformation: Application to medical image registration. J. Biomech. **40**, 919–929 (2007)
3. Holden, M.: A review of geometric transformations for nonrigid body registration. IEEE Trans. Med. Imag. **27**, 111–128 (2008)
4. Rueckert, D., Sonoda, L.I., Hayes, C. et al.: Nonrigid registration using free-form deformations: Application to breast MR images. IEEE Trans. Med. Imag. **18**, 712–721 (1999)
5. Schnabel, J.A., Tanner, C., Castellano-Smith, A.D.: Validation of nonrigid image registration using finite-element methods: application to breast MR images. IEEE Trans. Med. Imag. **22**, 238–247 (2003)
6. Wittek, A., Joldes, G., Couton, M. et al.: Patient-specific non-linear finite element modelling for predicting soft organ deformation in real-time; Application to non-rigid neuroimage registration. Progr. Biophys. Mol. Biol. **103** 292–303 (2010)
7. Miller, K., Wittek, A., Joldes, G. et al.: Modelling brain deformations for computer-integrated neurosurgery. Int. J. Numer. Meth. Biomed. Eng. **26** 117–138 (2010)
8. Paulsen, K.D., Miga, M.I., Kennedy, F.E. et al.: A computational model for tracking subsurface tissue deformation during stereotactic neurosurgery. IEEE Trans. Biomed. Eng. **46**, 213–225 (1999)
9. Miga, M.I.: Development and quantification of a 3D brain deformation model for model-updated image-guided stereotactic neurosurgery. PhD. thesis, Dartmouth College, Thayer School of Engineering, Hanover (1998)
10. Miga, M.I., Paulsen, K.D., Hoopes, P.J. et al.: In vivo modeling of interstitial pressure in the brain under surgical load using finite elements. ASME J. Biomech. **122**, 354–363 (2000)
11. Grosland, N.M., Shivanna, K.H., Magnotta, V.A. et al.: IA-FEMesh: an open-source, interactive, multiblock approach to anatomic finite element model development. Comput. Meth. Programs Biomed. **94**, 96–107 (2009)
12. Wittek, A., Hawkins, T., Miller, K.: On the unimportance of constitutive models in computing brain deformation for image-guided surgery. Biomech. Model. Mechanobiology **8**, 77–84 (2009)
13. Joldes, G.R., Wittek, A., Miller, K.: Cortical surface motion estimation for brain shift prediction. In: Computational Biomechanics for Medicine IV Workshop (MICCAI 2009). London, UK, p. 50–59 (2009)
14. Joldes, G., Wittek, A., Miller, K. et al.: Realistic and efficient brain-skull interaction model for brain shift computation. In: Computational Biomechanics for Medicine III (MICCAI 2008 Associated Workshop), p. 95–105 (2008)
15. Joldes, G., Wittek, A., Couton, M. et al.: Real-time prediction of brain shift using nonlinear finite element algorithms. Medical Image Computing and Computer Assisted Intervention (MICCAI 2009), London, LNCS 5762, p. 300–307 Springer, Berlin (2009)
16. Miller, K., Chinzei, K.: Mechanical properties of brain tissue in tension. J. Biomech. **35**, 483–490 (2002)
17. Miller, K., Joldes, G.R., Lance, D. et al.: Total Lagrangian explicit dynamics finite element algorithm for computing soft tissue deformation. Communications. In Numerical Methods in Engineering vol. **23**, 121–134 (2007)
18. Joldes, G., Wittek, A., Miller, K.: Computation of intra-operative brain shift using dynamic relaxation. Comput. Meth. Appl. Mech. Eng. **198**, 3313–3320 (2009)
19. Joldes, G.R., Wittek, A., Miller, K.: Suite of finite element algorithms for accurate computation of soft tissue deformation for surgical simulation. Med. Image Anal. **13**, 912–919 (2009)
20. Barber, C.B., Dobkin, D.P., Huhdanpaa, H.T.: The quickhull algorithm for convex hulls. ACM Trans. Math. Softw. 22, 469–483 (1996)
21. Gonzalez, R.C., Woods, R.E., Eddins, S.L.: Digital Image Processing using Matlab. Gatesmark Publishing (2009)

22. Schoenberg, I.J.: Contributions to the problem of approximation of equidistant data by analytic functions. Q. Appl. Math. **4**, 45–99 (1946)
23. Lee, S., Wolberg, G., Shin, S.Y.: Sacttered data interpolation with multilevel B-Splines. IEEE Trans. Visual. Comput. Graph. **3**, 228–244 (1997)
24. Wells III, W.M., Viola, P., Atsumi, H. et al.: Multi-modal volume registration by maximization of mutual information. Medical Image Analysis 1, 35-51 (1996)
25. Mattes, D., Haynor, D.R., Vesselle, H. et al.: Nonrigid multimodality image registration. In: Proceedings of SPIE 4322, 1609 (2001)
26. Fedorov, A., Billet, E., Prastawa, M. et al.: Evaluation of Brain MRI alignment with the Robust Hausdorff distance measures. In: The 4th International Symposium on Visual Computing 2008, LNCS, p. 594–603 (2008)
27. Canny, J.: A computational approach to edge detection. IEEE Trans. Pattern Anal. Mach. Intell. **8**, 679–698 (1986)
28. Garlapati, R.R., Joldes, G.R., Wittek, A., et al.: Objective evaluation of accuracy of intra-operative neuroimage registration. In: Computational Biomechanics for Medicine VII (MICCAI Associated Workshop) (accepted) (2012)
29. Ji, S., Fan, X., Roberts, D.W. et al.: Cortical surface strain estimation using stereovision. In: Medical Image Computing and Computer Assisted Intervention (MICCAI 2011), Toronto. LNCS 6891, p. 412–419 Springer, Berlin (2011)